Chapter 3: PIC Simulation, Magnetic and Thermal Tuning Studies of Millimeter-Wave Gyrotron

3.1. Introduction

In the preceding chapter, the non-linear behavior of the gyrotron is presented. The Multimode study has been made to investigate the beam-wave interaction phenomenon in the cavity. To investigate the effect of mode competition in the cavity, the Multimode analysis has been used, proving itself to be a very effective approach. Due to the incorporation of an arbitrary interaction structure and the non-homogeneity of the magnetic field, Multimode theories have been adopted for beam-wave interaction analysis of a gyrotron that employs a cylindrical open-ended cavity as an RF-interaction structure. The beam-wave interaction process is very complex, as it depends on several parameters that affect the performance of the gyrotron.

A computer code has been developed based on Multimode theory whose validity is established by verifying the results obtained from published results. To compare the Multimode code results, a millimeter-wave gyrotron operating at 260 GHz is chosen and studied for dynamic nuclear polarization / nuclear magnetic resonance (DNP / NMR) application. The Multimode code incorporates both design and electron beam parameters that are as similar to those used in the experimental 260 GHz gyrotron. In addition, particle-in-cell (PIC) simulations are also used to investigate the beam-wave interaction behavior of the device [106] – [107]. PIC simulations provide an insight into the device's electromagnetic behavior and helps in optimizing the structural and the beam parameters of the device that contribute to the finalization of the design of the cavity prior to fabrication. The device's proper scenario is realized by incorporating various practical constraints in the PIC simulation of the device.

The gyrotron has an open-ended tapered cavity, which is used as an RF interaction structure for beam-wave interactions in the cavity and produces RF radiation. Under cold conditions (in the absence of an electron beam), the RF interaction

structure has been investigated for the operating mode and frequency through the Eigenmode analysis. The device performance under practical condition, *i.e.*, under hot condition (in the presence of the electron beam) has also been appreciated for the gyrotron oscillator using different commercially available PIC codes. Some advanced simulation software, *e.g.*, MAFIA, MAGIC, and CST Studio Suite are commercially available to solve 3D particle-wave interaction problems. Using these simulation tools, the complex process of beam-wave interactions has been understood better.

The PIC solver module of "CST Particle Studio" is used to investigate the gyrotron's beam-wave interaction mechanism. The CST Particle Studio gives information about the mode competition in the cavity by observing the RF amplitude of operating mode as well as the RF amplitude of the competing modes in the time domain. The Fourier Transform of RF signals gives the frequency spectrum of the mode, which indicates its resonant frequency. In PIC simulations, the energy distribution of all particles along the interaction length is displayed to understand the energy transfer phenomena. The effect of velocity or energy spread on the device performance is discussed. The tapered cavity's overall device performance as its RF interaction structure has been observed in terms of output power.

The gyrotron has been proven to be the most attractive high power source at millimeter and sub-millimeter wave regimes [1]. Its applications are extended in recent years to novel high-frequency spectroscopy, including electron paramagnetic resonance (EPR), and nuclear magnetic resonance (NMR) with the enhancement of signal strength by using dynamic nuclear polarization (DNP) technique at high magnetic field [3]. The detailed discussion on DNP / NMR has been already given in Chapter – 1. To achieve broad frequency tuning, gyrotrons are normally operated in higher-order axial modes by varying applied magnetic fields known as magnetic tuning schemes. In a continuous

wave (CW) gyrotron, the RF cavity's thermal deformation is an undesired problem that arises from the ohmic loss caused by its finite wall conductivity. Taking advantage of thermal deformation due to ohmic loss in the RF cavity, the frequency tuning of gyrotrons can further be enhanced by controlling the thermal deformation of the RF interaction cavity [108]–[110], which is known as thermal tuning scheme.

In the present chapter, the modeling and simulation investigations of a low power millimeter wave gyrotron operating in $TE_{7,2}$ mode at ~260 GHz are carried out to achieve improved tunable bandwidth using a magnetic tuning scheme. Section 3.2 deals with the descriptions of PIC simulation. Section 3.3 deals with the modeling and 3D PIC simulation of beam-wave interaction of millimeter-wave gyrotron. The thermal and structural analyses of the RF cavity are performed for observing the deformation of the cavity and its effect on the resonant frequency of gyrotron in section 3.4. The magnetic tuning and thermal-frequency-tuning techniques are investigated in section 3.5. The RF window and collector are discussed in section 3.6. Finally, conclusions are drawn in section 3.7.

3.2. Descriptions of PIC Simulation

CST Microwave Studio is a Finite Integration Technique (FIT) based simulation tool. Eigenmode Solver is used to observe the mode pattern, vector plot, contour plot, and the electric field intensity in the cavity in the case of lossless resonant structure. The Eigenmode solver provides the quality factor using the perturbation method and the structure's resonant frequency. The Eigenmode solver cannot be used with open boundaries or discrete ports [111]. CST particle studio is used to investigate the beam-wave interaction behavior in the cavity. It uses hexahedral/tetrahedral meshing in simulations for the discretization of computational areas.

To diagnose the results obtained, the post-processing module is the salient feature of the simulation tool. CST Particle Studio has a provision to monitor RF signal amplitude for more modes at the output port. After defining the RF interaction structure's geometry, a cathode surface is also defined at the open end of the down taper. The circular particle emitter is placed on the cathode's surface, which concentrates along the axis of the cavity. Here, a DC beam emission model is selected, which requires the particles to assign any constant value parameter as the Lorentz factor (γ), normalized velocity (β), velocity (v), or energy (U), and pitch factor (velocity ratio) α. These parameters can be calculated as follows,

$$\gamma = 1 + \frac{eV_b(kV)}{511} \tag{3.1}$$

$$\beta = \left[1 - \frac{1}{\gamma^2}\right]^{1/2} \tag{3.2}$$

$$v = \beta c = \left[v_z^2 + v_t^2\right]^{1/2} \tag{3.3}$$

$$U = (\gamma - 1)\left(m_e c^2 / e\right) \tag{3.4}$$

$$\alpha = \frac{v_t}{v_z} \tag{3.5}$$

Where, v_b is the beam voltage, v_z and v_t are the axial and transverse velocities of the particle, respectively, m_e is the rest mass of the electron and 'c' is the velocity of light. The velocity spread is introduced in the present simulation based on the Magnetron Injection GUN design (MIG). In addition, a waveguide port is defined at the open end of the upper part of the cavity to determine the RF signal amplitude of the operating mode as well as the competition mode.

Before running the simulation in CST Particle Studio, it is important to define four major steps: background, structure, frequency range, and boundary conditions. The

background is taken as normal and the frequency range is defined around the operating frequency. The boundary conditions are applied to all six faces of the bounding box. In PIC simulations, the tangential electric field $E_t = 0$ is applied to all the bounding box faces, as shown in Figure 3.1. Both E-field and H-field monitors are used to obtain the electric and magnetic field intensities, respectively, and mode pattern in the cavity at a particular frequency. The field monitor provides the resonating mode information at a particular frequency, and the resonating mode may be a co-rotating or counter-rotating. If the mode pattern is rotating in the anti-clockwise direction, then the mode is said to be co-rotating otherwise counter-rotating. The hot field profile of the cavity can be observed using the post-processing of the tool's field monitoring feature. The particles are monitored in either 2D or 3D plane to have information about the perturbation of particles in terms of energy or phase. The particle monitor (phase-space monitor) is used to calculate the speed, energy, and Lorentz factor (γ) at certain intervals of time along the axial length of the cavity.

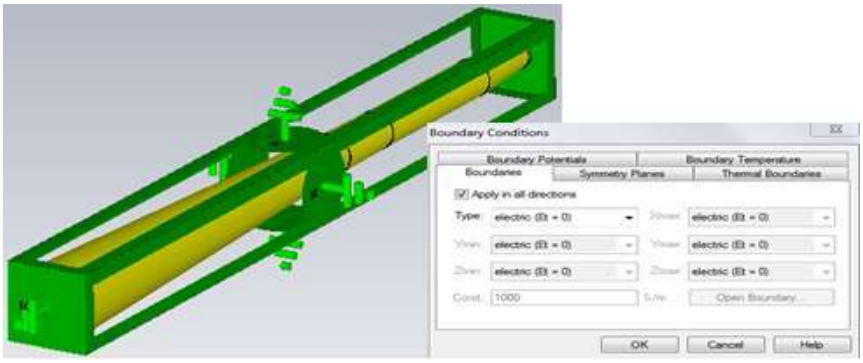

Figure 3.1 Boundary conditions implementations around the RF interaction cavity.

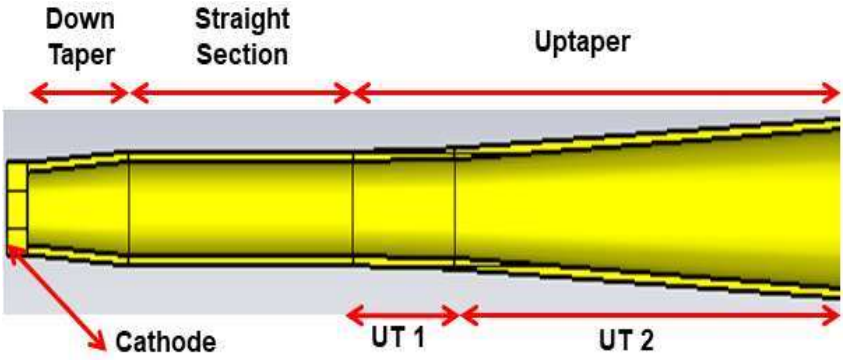

Figure 3.2 CST model of the gyrotron cavity.

3.3. PIC Simulation Gyrotron Cavity

3.3.1 Modeling and Beam-Wave Interaction Process

In order to investigate the beam–wave interaction phenomena and transient response of the gyrotron, the RF interaction cavity is modeled using annealed copper with reduced conductivity as, $\sigma = \sigma_{Cu}/2 = 2.9 \text{ X}10^{7}$ S /m in a commercially available Finite Integration Technique (FIT) based "CST Particle Studio". The design parameters are given in Table – 2.1. The CST model of the RF interaction cavity is shown in Figure 3.2. In the present hot simulation, a total of 144 emission points are considered in the cathode surface with hexahedral meshing. In the present PIC simulation the DC beam values, V_b = 15.5 keV, I_b = 100 mA, B_o = 9.515 T and α = 1.12 and velocity spread ~2 % are used. Initially, all beamlets' Larmor radii and energy have remained the same as ~1.374 mm and ~15.5 keV (left side intensity bar of Figure 3.3), respectively. At the output side, the Larmor radii and energy of all beamlets are modulated due to the RF wave's perturbation as shown in Figure 3.3 (right side of the intensity bar). The change in Larmor radii and cyclotron frequency of electrons leads to the phase bunching of electrons. Once the electrons' bunching takes place, some of the electrons transfer their kinetic energy to the RF field.

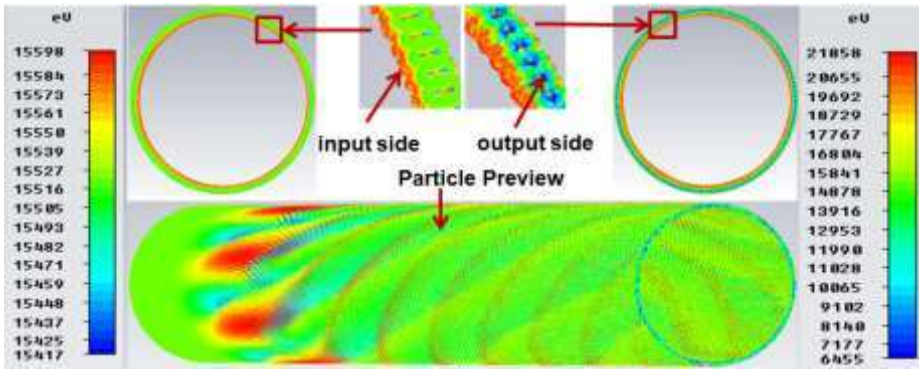

Figure 3.3 Particle preview of electron beam at the input side and at the output side.

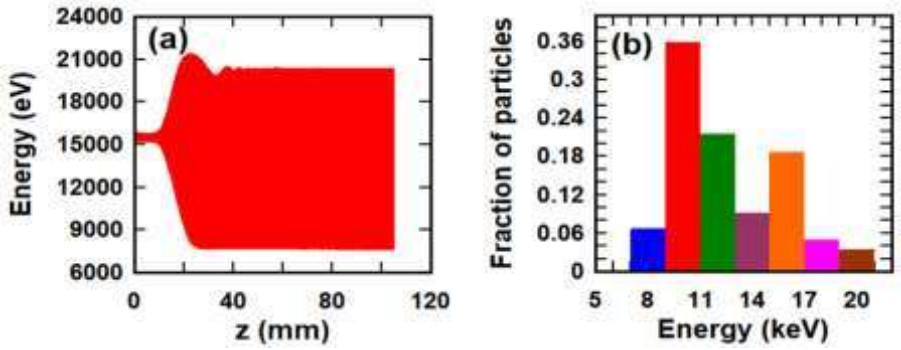

Figure 3.4 (a) Particle energy of the electron beam (b) fraction of the particle energy.

3.3.2 PIC Simulation Results

The particle energy distribution along the axial length of the cavity is shown in Figure 3.4 (a). The distributions of the normalized fraction of particles with respect to their energy are shown in Figure 3.4 (b). It is observed that at the input side of the RF interaction cavity [z = 0 mm, Figure 3.4 (a)]; the average particle energy is around ~15.5 keV. After the beam-wave interaction process, the majority of particles [Figure 3.4 (b)] have lost their energy and transfer to the RF wave. As a result, a temporal growth of the RF signal takes place at the output port. The total 2 % velocity spread is considered in the PIC simulation. The present PIC simulation of conventional gyrotron generated an RF output signal [Figure 3.5 (a)] at the output port in the desired operating $TE_{7,2}$ mode and other competing modes including $TE_{2,4}$, $TE_{11,1}$, and $TE_{4,3}$ modes. The post-processing of the signal shown in Figure 3.5 (a) results a CW peak power [Figure

3.5 (b)] in $TE_{7,2}$ mode as ~150W at the resonant frequency of ~260.46 GHz [Figure 3.5 (c)]. Further, the simulated output is validated using a time-dependent nonlinear Multimode theory [91]. The Multimode code predicted a maximum RF power as ~165W with no velocity spread in the desired operating $TE_{7,2}$ mode and negligible power in other competing modes [Figure 3.5 (d)]. The Multimode response is in good agreement with the obtained 3D beam-wave interaction simulation results.

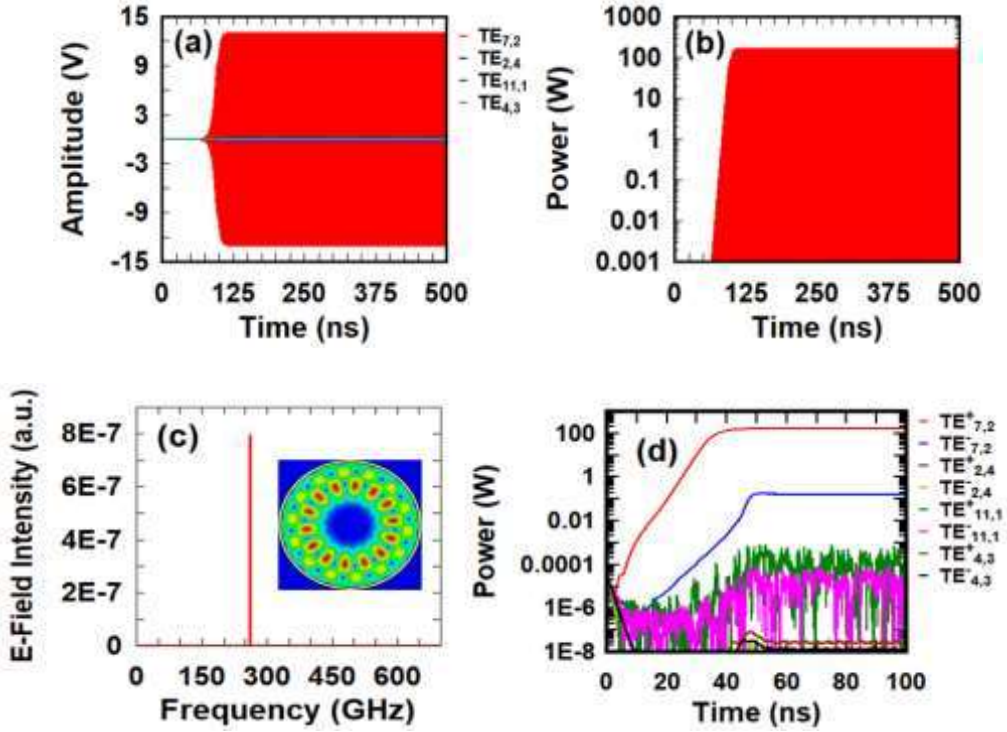

Figure 3.5 (a) Amplitude of port signals, (b) power of $TE_{7,2}$ mode, (c) frequency spectrum of the port signal of $TE_{7,2}$ mode and (d) theoretically calculated power.

Table 3.1: Properties of OFHC-Cu material at 290 K [112]

Properties	Value
Density (Kg /m^3)	8978
Thermal conductivity (W /m-K)	390
Specific heat (J /Kg-K)	385
Emissivity	0.4
Elastic modulus (GPa)	120
Thermal expansion coefficient (μm C^{-1})	17
Poisson's ratio	0.33

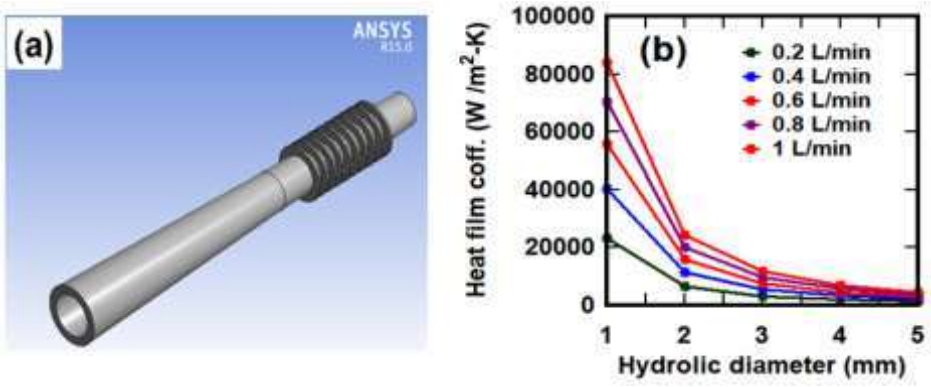

Figure 3.6 (a) ANSYS model of the RF interaction cavity, (b) Heat transfer coefficient with a hydraulic diameter for different water flow rates in the grooves.

3.4 Thermal Study of Gyrotron cavity

The present conventional gyrotron cavity is modeled in the Finite Element Method (FEM) based commercially available ANSYS [113] for studying its thermal and structural behaviors. The cavity is designed using copper with reduced conductivity as $\sigma = \sigma_{Cu}/2 = 2.9 \times 10^7$ S/ m. The other properties of OFHC-Cu are given in Table – 3.1. The wall loading (ohmic loss) in the cavity is calculated as [109], [114],

$$\frac{dP}{dA} = \frac{2\pi\delta}{\lambda^2} \frac{P_{out} Q_d}{\chi_{m,n}^2 - m^2 \; L} \tag{3.6}$$

where, λ is the operating wavelength, $\chi_{m,n}$ = 12.927 for $TE_{7,2}$ mode, L is the length of interaction cavity (straight section), m is the azimuthal index, n is the radial index, and $\delta = \sqrt{2/\sigma\omega\mu}$ is the skindepth. The skindepth is calculated as ~1.83 $\times 10^{-7}$ m at 260.46 GHz. Q_d is the diffractive quality factor which is given by $4\pi \; L/\lambda \;^2 \Big/ \; 1 - R_1 R_2$, where R_1 and R_2 are the electric field reflection coefficient at both ends of the cavity, respectively. The diffractive quality factor is calculated as ~12,240. The ohmic quality factor (Q_{ohm}) is given by $\left(R_o/\delta\right)\left(1-\left(m^2/\chi_{m,n}^2\right)\right)$, where R_o is cavity radius [1]. The Ohmic loss [1] is calculated as ~650 kW /m^2 for the diffractive quality factor of

~12,240. The ANSYS model of the RF interaction cavity with grooves is shown in Figure 3.6 (a). To reduce the temperature in the cavity section, radial grooves are used and in which water coolant is passed at 290 K. The heat is flowing from the inner surface to the outer surface via conduction and the outer surface to the coolant via convection. The dissipated power (Ohmic loss) is used as heat flux in the simulation. The heat flux (wall load) is applied on the inner surface of the straight section of the cavity. The thickness of the cavity and grooves are optimized as 2 mm and 1 mm, respectively. The radial fins (grooves) on the outer surface of the cavity are used to reduce the thermal loading that provides the stable operation of the gyrotron. The spacing between the grooves and the height of the grooves is optimized as ~2 mm. A total of 10 grooves are used on the surface of the cavity. The total amount of water flowing between grooves is at the rate of ~7 L /min, which is directly exposed to the outer surface of the RF interaction cavity. The thermal conductivity, Prandtl number, density, specific heat and viscosity of water (inlet) are considered as ~0.6 W /m – K, 6.99, ~998.2 kg /m^3, ~4182 J /kg-K, and ~0.001003 N.s /m^2, respectively, at 290 K. 3D steady state and absolute velocity formulations are used in the Fluent Solver of ANSYS. The $\kappa - \varepsilon$ turbulence model with enhanced wall treatment is chosen for estimating the pressure gradient near the water-copper wall regions. The wall boundary-loaded heat flux distribution on the inner surface of the cavity is chosen as boundary condition with fine meshing in the present thermal study. Velocity – inlets for the inlet surface, pressure-outlet for the outlet surface are considered in the simulation and the default boundaries are selected for other surfaces. The variation of heat transfer coefficient [109], [114] with respect to the hydraulic diameter for various water flow rate is shown in Figure 3.6 (b). The average heat transfer coefficient of water-cavity surface is calculated as ~15500 W /m^2–K by using post-processing of the simulation.

The cavity is simulated in the Fluent Solver and Static Structural Solver of ANSYS, which gives the temperature distribution and structural deformation of the cavity. The resonant frequency of gyrotron is very sensitive to the straight cavity section's inner radius that depends on the temperature inside the cavity and the corresponding deformation. The temperature at the inner surface of the straight cavity section and the corresponding deformation is observed for various water [at coolant temperature (T.C.) 290 K] flow rate [Figure 3.7 (a)]. In the thermal analysis, the water flow rate is chosen as ~3m /s, beyond which the temperature and deformation at the inner surface of the cavity are almost constant [Figure 3.7 (a)]. The resonant frequency of the cavity and the shift in resonant frequency with respect to water flow rate are calculated using Eigenmode solver [Figure 3.7 (b)]. It is observed that the resonating frequency decreases as temperature increases, hence the frequency shift increases. The average temperature at the inner and outer surfaces is observed as ~308 K and ~303 K, respectively [Figure 3.8 (a)]. The average radial deformation in the straight cavity section's radius after fixing both ends of the cavity is observed as ~0.61μm [Figure 3.8 (b)]. The average temperature at the cavity's inner surface is observed as ~298 K only when the coolant temperature is 280 K on the surface of the cavity. At this coolant temperature, negligible deformation is observed in the RF cavity resonating at ~260.46 GHz. As the coolant temperature is 290 K, the cavity's resonant frequency is shifted to ~260.39 GHz. Therefore, the net frequency shift is only ~70 MHz. The shift in resonant frequency enhances the tuning range of the gyrotron.

3.5 Continuous Frequency Tuning of Millimeter-Wave Gyrotron

The most important advantage of gyrotrons is the possibility of tuning their frequency by changing the magnetic field. The smooth transition between the higher-

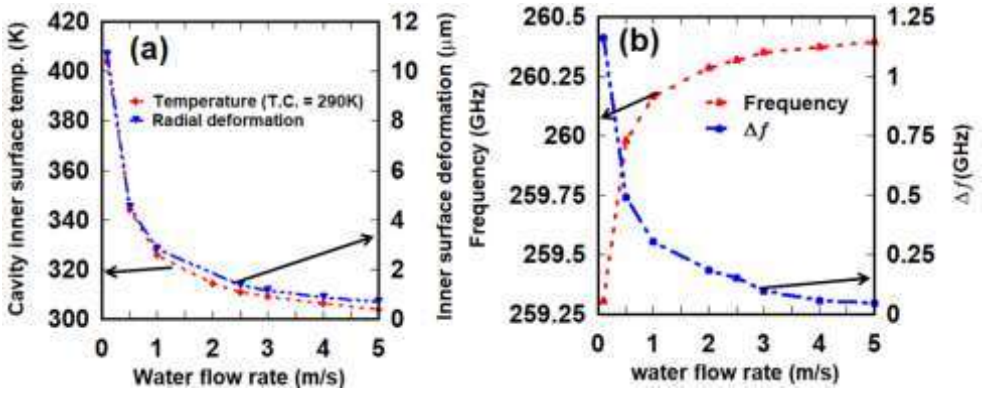

Figure 3.7 (a) The temperature and deformation of the inner surface of straight section of the cavity, (b) the resonating frequency with respective water flow rate and shifting in resonating frequency at corresponding water flow rate at 290K.

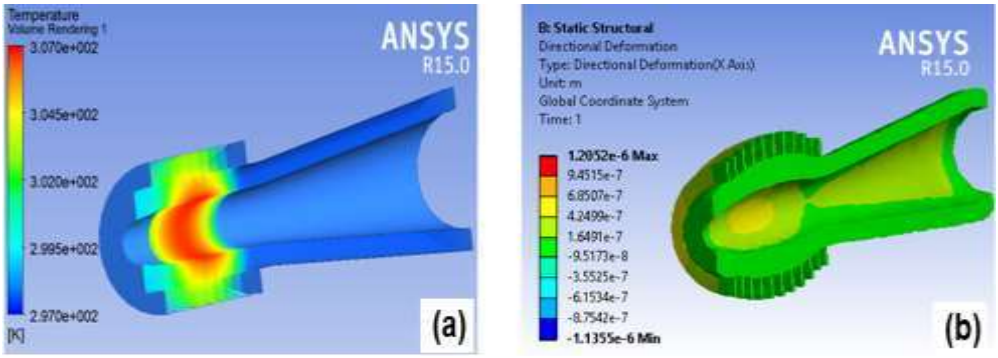

Figure 3.8 (a) The temperature distribution in the cavity, and (b) the total deformation of the cavity at coolant temperature 290K.

order axial modes (HOAMs) allows smooth and continuous frequency tuning of gyrotron frequency. The excitation of HOAMs can be explained by using an underlying theory of the closed cylindrical cavity. The spectrum of the resonant frequency of a closed cylindrical cavity for $TE_{m,n,q}$ mode is given by $\omega_{m,n,q} = c\sqrt{k_{\perp m,n}^2 + k_{z,q}^2}$, where, $K_{\perp,m,m} = \chi_{m,n}/R_o$ and $k_{z,q} = q\pi/L_c$ are the transverse and axial wavenumbers. Since the $\chi_{m,n}$ and q can take only discrete values so the spectrum of such cavities is also discrete. In practice, the gyrotron cavity is open at both ends to allow an electron beam to enter the resonant structure from one side and leave it from the other side. Therefore, the spectral properties of open-ended and slightly tapered cavities are slightly different

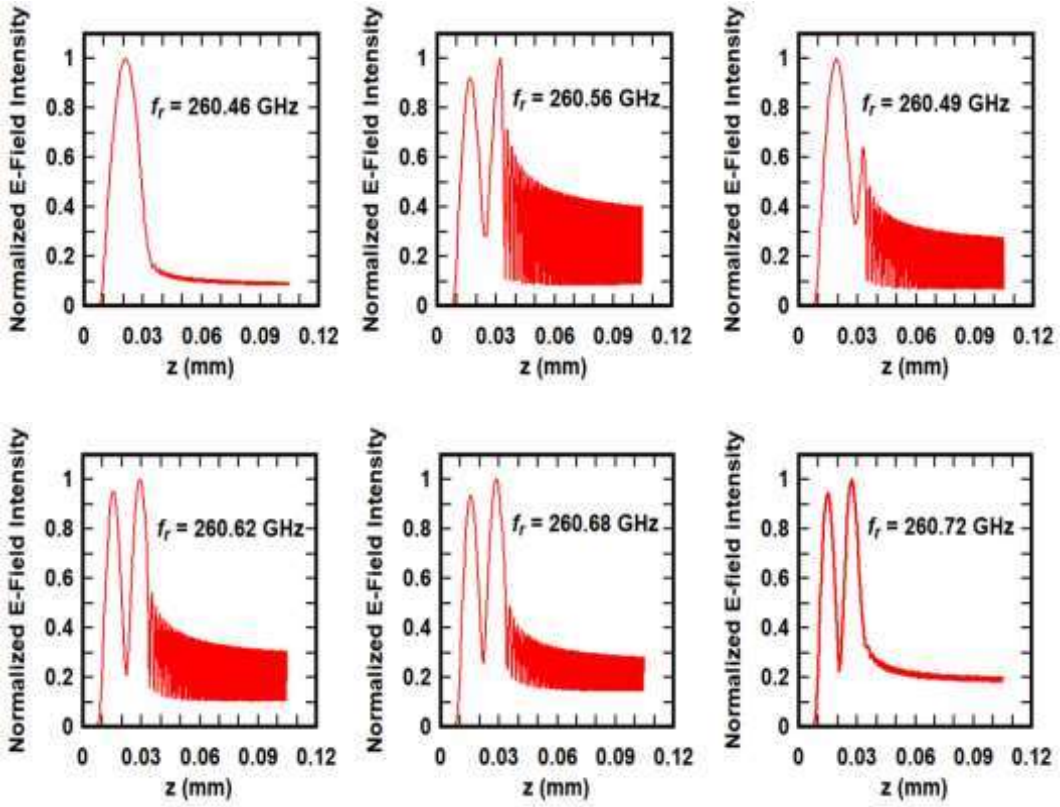

Figure 3.9 The smooth transition between the q = 1 –like mode and q = 2 –like mode.

from the closed cavity. The resonance in open cavities is quasi-normal modes (QNM) with complex frequencies in order to account for the cavity losses and output coupling. Therefore, the spectrum of open-ended cavities is defined by the corresponding Eigenvalue problem of the Helmholtz's equation (2.86) with specific boundary condition (2.87) at both ends of the cavity, as given in Chapter – 2. The longitudinal axial profiles in the open-ended cavities are like profile (q = 1 –like, 2 –like profile). So, effective axial mode number (q) may not be an integer. The smooth transition between q = 1 –like mode to q = 2 –like mode is obtained by varying the magnetic field, as shown in Figure 3.9.

The steady-state operation of gyrotron is achieved by optimizing the beam voltage (V_b), beam current (I_b), pitch factor (α), and magnetic field (B_c). The operating frequency of gyrotron depends upon the cavity radius (R_c) and the cyclotron

Table 3.2: Quality factors and f_r for axial mode number (q = 1 – 6)

q	Frequency (GHz)	Q_d	Q_T
1	260.46	12420	5266
2	260.69	3030	2276
3	261.05	1290	1130
4	261.57	690	641
5	262.24	416	397
6	263.5	260	252

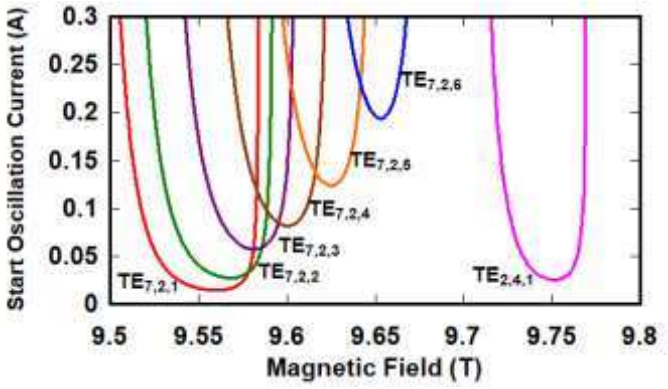

Figure 3.10 SOC for axial mode number q = 1 – 6.

angular frequency $\left(\omega_c = eB_c/\gamma m_e\right)$ should be less than the operating frequency, where, 'e' is electron mass, B_c is applied external magnetic field and γ $\left(\gamma = 1 + \frac{V_b(keV)}{511}\right)$ is the relativistic factor. Therefore, the resonant frequency of gyrotron can be changed by controlling γ, B_c, and R_c. The frequency tuning in gyrotron can be achieved in three ways: (i) electrical tuning by varying the beam voltage (V_b), (ii) magnetic tuning by varying the magnetic field, and (iii) thermal tuning by controlling the thermal expansion of the cavity. In the present study, magnetic tuning and thermal tuning are performed to achieve gyrotron's tuneability.

3.5.1 Magnetic Tuning Scheme

In the present work, the magnetic tuning is chosen because the magnetic tuning is comparatively good as the electron cyclotron angular frequency (ω_c) is directly proportional to the applied magnetic field (B_o) that can change the cyclotron frequency

more effectively than the voltage tuning. An axially long cavity reduces the SOC [Figure 3.10], hence a series of axial modes can be excited in the cavity. Thus, some higher-order axial modes like $TE_{m,n,q}$ are excited in the cavity, where, q is greater than one. The higher-order $TE_{m,n,q}$ ($q > 1$) axial modes are excited in the cavity just above the magnetic field at which $TE_{m,n,1}$ is excited and these modes resonate at higher frequencies. Therefore, a broad continuous frequency tuning is obtained. The shifting in resonating frequency $(\Delta\omega)$ during magnetic tuning can be estimated by [115]

$$\frac{\Delta\omega}{\omega} \approx \frac{1}{8}\left(\frac{\lambda}{L}\right)^2 \left(q^2 - 1\right) \tag{3.7}$$

where Δω is the shift in resonating frequency, ω is the cavity Eigen frequency, L is the length of the straight section of the cavity, λ is operating wavelength and q is the axial mode number. The diffractive (Q_d) and total quality factors (Q_T) are calculated for various axial mode numbers (q) of the operating $TE_{7,2,q}$ mode, which is given Table – 3.2. The tuning range of mode numbers, q = 1 – 6, are realized by varying the magnetic field [116]. It shows that $TE_{7,2,q}$ mode for q = 1 – 4 can be excited in the magnetic tuning range of ~9.51T to ~9.71T with the output power of more than ~1.5 W. The cavity field profile for axial index number q = 1 – 4 are calculated at the respective frequency, as shown in Figure 3.11 (a) – (d). The E-field monitor spectrum is observed at 260.46 GHz, 260.69 GHz, 261.05 GHz, and 261.57 GHz corresponding to the axial index number q = 1, 2, 3, and 4, respectively, as shown in Figure 3.12 (a) – (d). However, while tuning the gyrotron for a broad range, its output power is decreased [Figure 3.13 (a)], due to the abrupt change in 'Q_d' at higher-order axial mode number of operating mode. In the present simulation, a magnetic tuning of ~1.3 GHz (260. 46 GHz

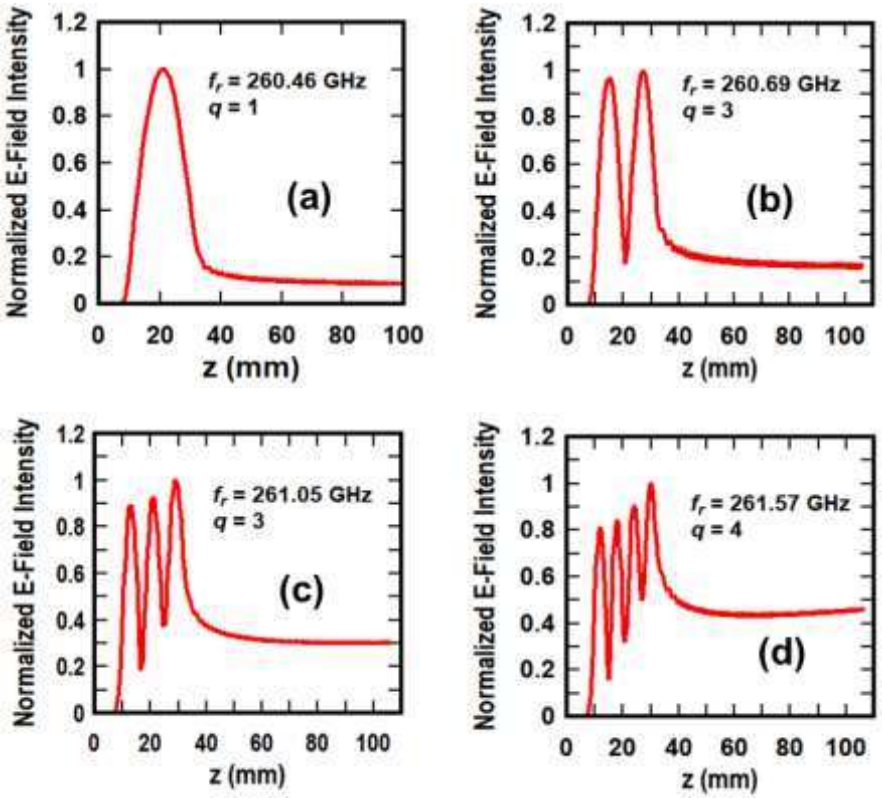

Figure 3.11 The cavity field profile for axial mode number q = 1 – 6.

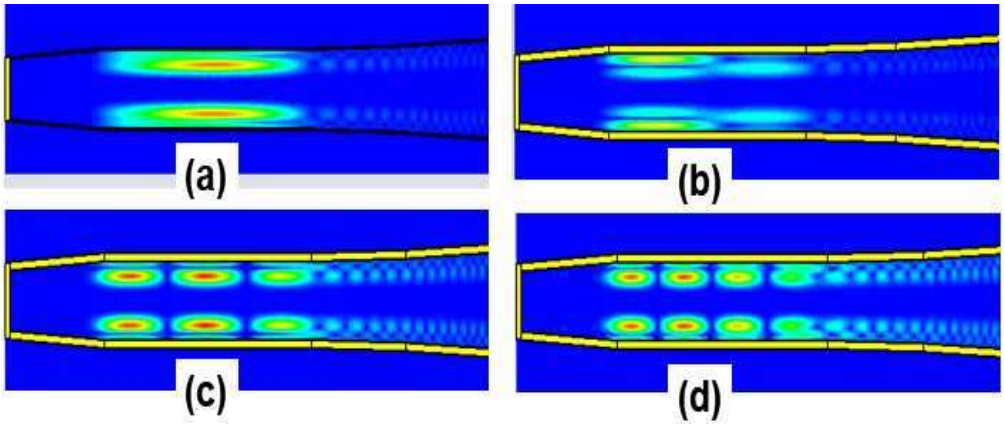

Figure 3.12 The spectrum of the E-field monitors at the frequency (a) 260.46 GHz, (b) 260.69 GHz, (c) 261.05 GHz, and (d) 261.57 GHz.

– 261.76 GHz) is observed for q = 1 – 4 [Figure 3.13 (b)] while the coolant temperature is 280 K on the outer surface of the cavity. Further, the cavity is simulated at various velocities spread (0 %, 2 %, and 4%). However, it shows the very nominal variation in the output power, as predicted in Figure 3.14. PIC simulation results are validated using

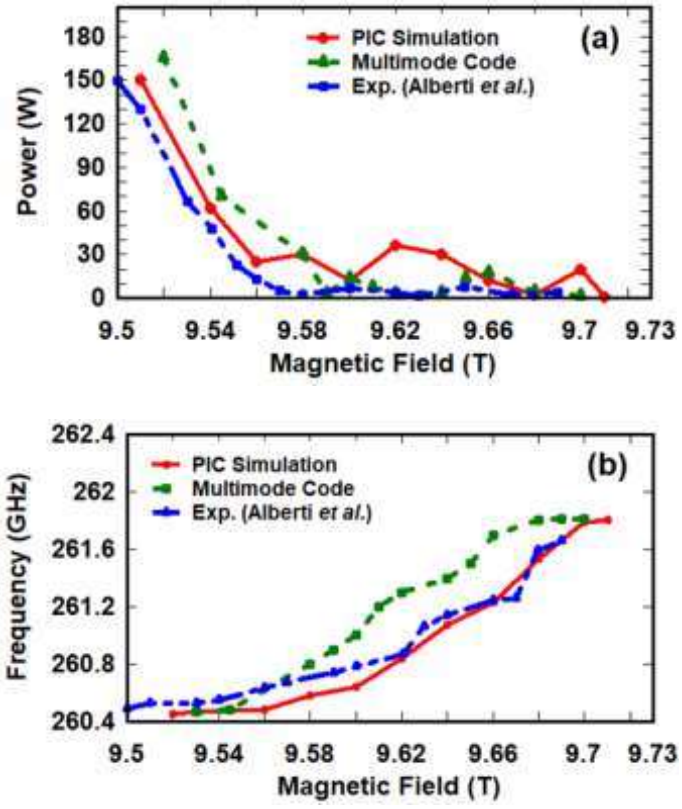

Figure 3.13 (a) Power Vs magnetic field (b) resonating frequency with the respective magnetic field (beam parameters are 15.5 kV, 100 mA, α = 1.12, and total velocity spread is 2%).

a time-dependent multi-mode code and found that they are in good agreement. The present theoretical observations are also found that they are in close agreement with an experimentally tested millimeter-wave gyrotron by Alberti *et al.* [65], as shown in Figure 3.13 (a) and Figure 3.13 (b), respectively.

3.5.2 Thermal tuning Scheme

Thermal tuning is another technique to enhance the tunable bandwidth further. In the present analysis, the groove's shape and the velocity of the coolant between the grooves are taken to be similar to the groove size and velocity of the coolant given in the previous section 3.4. The structural deformation of the RF cavity is controlled by varying the coolant's temperature that is flowing through the channel on its outer surface. The radial deformation is observed by fixing both ends of the cavity.

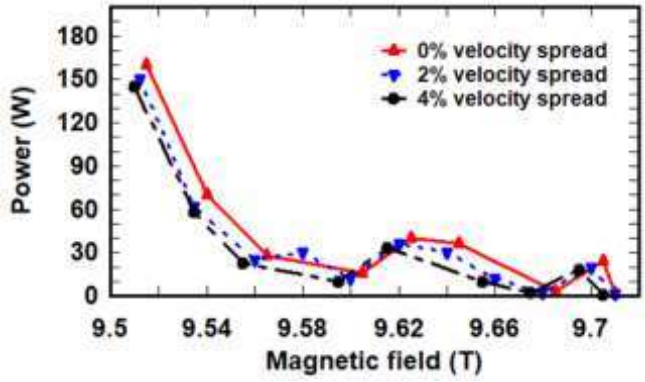

Figure 3.14 Power Vs magnetic field for various velocity spread (beam parameters are 15.5 kV, 100mA, and $\alpha = 1.12$).

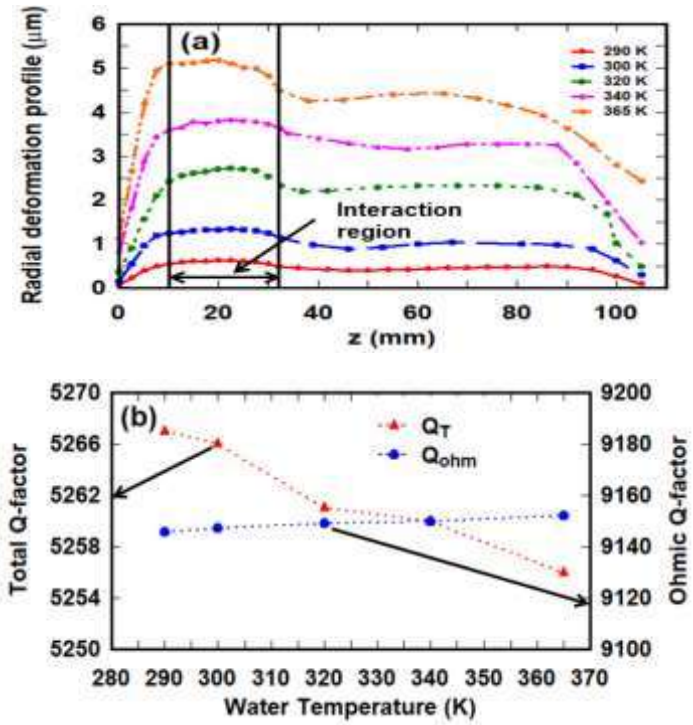

Figure 3.15 (a) Deformation distribution in the cavity and (b) The total quality factor (Q_T) and ohmic quality factor (Q_Ω) at the respective temperature.

The frequency tunability of gyrotron is investigated at various coolant temperatures, including 290K, 300K, 320K, 340K, and 365K while keeping other electrical parameters constant. As the effective radius of the cavity increases with respect to the coolant temperature, the cavity's cut-off frequency decreases. To maintain the stable operation and achieve high efficiency of gyrotron that should be operated in single-mode and very close to its cut-off frequency of the cavity. Since the cyclotron angular

frequency in gyrotron is more sensitive to the applied DC magnetic field, synchronization with the operating frequency is difficult. In the magnetic tuning, the gyrotron responds very quickly. Its CW output is very low (< 1.5W) at a higher magnetic field or higher axial mode number of the operating mode. Since the gyrotron's output power is limited by the axial mode number of the cavity, its tuneability is also limited for fixed electrical parameters. The average deformation in the inner radius of the straight cavity section [Figure 3.15 (a)] at 290K, 300K, 320K, 340K, and 365K is observed as ~0.61μm, ~1.3μm, ~2.72μm, ~3.85μm, and ~5.13μm, respectively. The corresponding resonating frequency due to cavity deformation is observed as ~260.39GHz, 260.31GHz, 260.18GHz, 260.05GHz, and 259.88GHz, respectively. Therefore, the maximum shift in resonant frequency is ~0.58GHz with respect to the obtained resonant frequency of regular (without deformation) cavity at 280K of coolant temperature. The quality factor (Q) of the cavity is also sensitive to the radius of the cavity. The Ohmic Q factor (Q_Ω) and total Q factor (Q_T) are calculated with respect to the deformation at the respective coolant temperature [Figure 3.15 (b)]. Further, as the coolant temperature is increased the output power is shifted towards the lower side of the magnetic field [Figure 3.16 (a)], because the operating frequency decreases with respect to the coolant temperature [Figure 3.16 (b)]. The thermal tuning scheme is advantageous over the magnetic tuning scheme because the average output power obtained in thermal tuning is higher than that obtained from magnetic tuning. The reason for high average output power in thermal tuning range is that the gyrotron is operated in the axial mode number of q = 1 only. Still, in magnetic tuning, the gyrotron is also operated in higher-order axial mode numbers, *i.e.*, q = 2, 3, etc. The working mechanism of thermal and magnetic tunings is different; therefore the effect of both

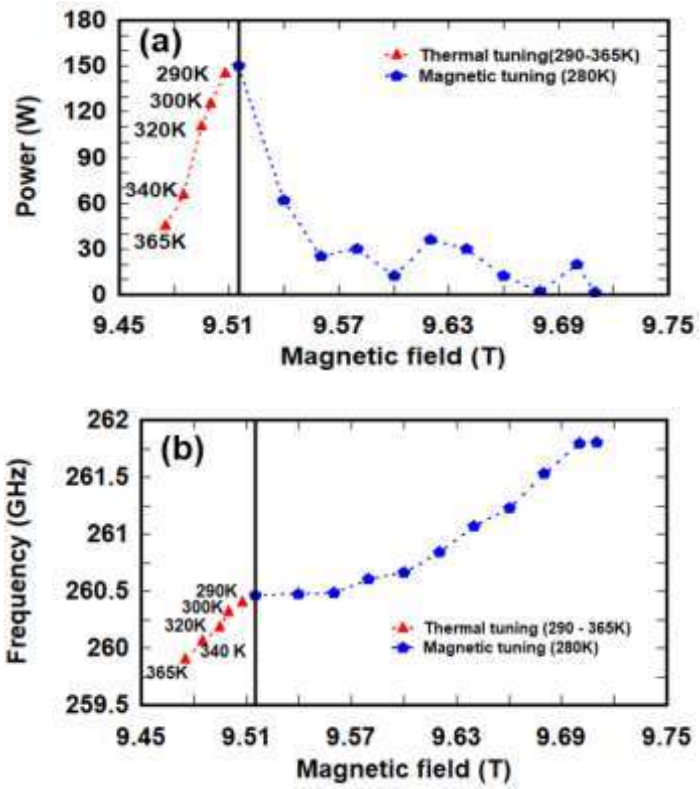

Figure 3.16 (a) Power versus magnetic field for thermal tuning and magnetic tuning and (b) Frequency versus magnetic field for thermal tuning and magnetic tuning.

tuning schemes is combined for obtaining higher tuning bandwidth. The tunable bandwidth is obtained as ~0.58 GHz from the thermal tuning scheme alone in the present case.

3.6 Output System of the Gyrotron

3.6.1 RF Output Window

The output window is an important part of the gyrotron oscillator, which extracts the developed RF power and couples to the external system. The window must be designed in such a way that it can bear the thermal and mechanical stresses. A single disk window is considered in the present case. In a simple single disk window, waveform reflection reaches a minimum only as the window thickness (d) becomes equal to the integral number of half-wavelengths for the main (disk) medium. The

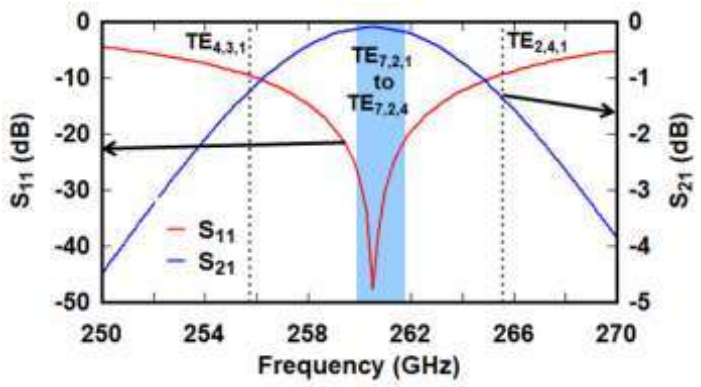

Figure 3.17 Transmission and reflection characteristics of single disk Sapphire window at $\varepsilon_r = 9.394$ and loss tangent $\tan(\delta) = 4.5 \times 10^{-4}$.

reflectance (R_p, relative to the power) or reflection coefficient (S_{11}) of the single disk window is given by [117],

$$R_p = |S_{11}|^2 = \frac{(1-\varepsilon_r)^2 \sin^2\left(\frac{2\pi d\sqrt{\varepsilon_r}}{\lambda}\right)}{4\varepsilon_r + (1-\varepsilon_r)^2 \sin^2\left(\frac{2\pi d\sqrt{\varepsilon_r}}{\lambda}\right)} \tag{3.8}$$

where ε_r is the relative permittivity of the material (disk) and λ is the operating wavelength. The present single disk window is designed by using Sapphire material ($\varepsilon_r = 9.394, \tan\delta = 4.5 \times 10^{-4}$) having ~ 40 mm diameter and thickness of $4\lambda/2 = 0.75$ mm are designed, where, λ is the wavelength in Sapphire material at 260.5 GHz [64]. The absorption coefficient of the single-disk window is given by [118],

$$A_b = \pi d(1+\varepsilon_r)\tan(\delta)/\lambda \tag{3.9}$$

The reflection and absorption coefficients are calculated by using equations (3.8) and (3.9), respectively. The absorption coefficient for the Sapphire window is estimated at ~0.98 % at 260.5 GHz. The transmission coefficient (S_{21}) is calculated by using $|S_{21}|^2 = 1 - |S_{11}|^2 - A_b$ [1]. The transmission and reflection characteristics of the output – window are plotted analytically, as shown in Figure 3.17. The numerical computation predicted the reflection and transmission coefficients as –47.58 dB and –0.043 dB,

respectively, at 260.5 GHz. These characteristics show that the Sapphire window is more transparent for $TE_{7,2,1}$ – $TE_{7,2,4}$ modes in the frequency tuning range ~259.9 GHz to ~261.8 GHz as compared to $TE_{4,3,1}$ mode at ~255.73 GHz and $TE_{2,4,1}$ mode at ~265.58 GHz.

3.6.2 Electron Beam Depressed Collector

The electron beam is generated at the cathode with accelerating voltage V_b. After the beam-wave interaction process, some fraction of the electron beam's energy is transferred to the RF wave and the spent electron beam is collected at the collector. To dump the electron beam at the collector electrostatically, the magnetic field must be reduced less than 0.01 T in the collector region. The electron beam radius in the collector is given by [1],

$$R_{bcoll} = R_b \times \sqrt{\frac{B_{cav}}{B_{zcoll}}} \tag{3.10}$$

where, R_{bcoll} and R_b are the beam radii in the collector and resonant cavity, respectively. B_{cav} and B_{zcoll} are the magnetic fields in the resonant cavity and collector, respectively. The collector's radius is estimated as ~43 mm in such a way that the thermal loading not exceed ~0.5 kW /cm^2. The Larmor radius (r_L) of electron beam-lets in the collector region is given by [1],

$$r_{L\ \max} = 0.11(mm) \times [V_b\ keV]^{1/2} / \ B\ (T) \tag{3.11}$$

where, $r_{L,max}$ is the Larmor radius in the collector, V_b is the beam voltage and B is the magnetic field in the collector region. The Larmor radius in the collector is estimated as ~44 mm. The axial beam width is related to radial beam width (generally $2\times r_L$) in the collector region and the electron beam angle at the collector surface. The axial beam width is calculated as ~88 mm, thus the surface area for heat load at the inner surface of

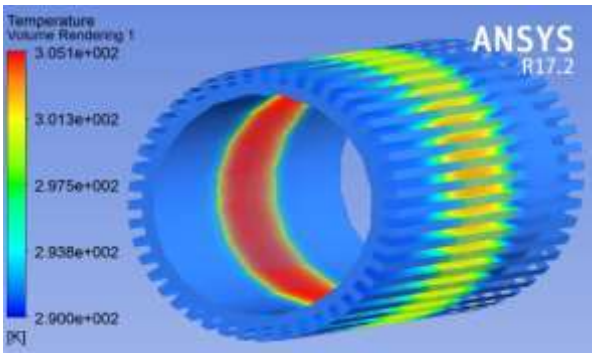

Figure 3.18 The temperature distribution of the collector.

the collector is 237.75cm^2 (2π×43×88 mm^2). Therefore, the maximum power density at the inner surface of the collector is calculated as ~6 W /cm^2 only for the output power ~150 W. The total length of the collector (~264 mm) is proposed as three times of the considered length of axial width of the electron beam, in which the axial beam width lies in the middle of the collector [119]. The present case's heat load is calculated as ~6 W /cm^2 by considering RF output power ~150 W and the depressed potential applied is –5 kV [120]. The collector is modeled using OFHC-Cu in ANSYS with the conductivity ~2.9 ×10^7 mho /m. The axial grooves are used to cool down the collector in the Fluent Solver. The grooves' height and width are optimized as ~4 mm and ~2 mm, respectively. The thermal and structural analyses are performed using the Fluent Solver and Static Structural solvers, respectively. The temperature at the inner and outer surfaces of the collector [Figure 3.18] is calculated as ~305 K and ~290 K, respectively, while the flow rate of water is ~0.7 L /m between the grooves at temperature 290 K. The overall efficiency of the gyrotron is enhanced from 9.67% to 14.27% while considering ~5 kV potential difference between the collector and the cavity [1].

3.7 Conclusion

In the present chapter, a millimeter-wave gyrotron cavity was modeled in “CST Particle Studio” to operate in $TE_{7,2}$ mode at 260 GHz. PIC simulations have been

performed to investigate the beam-wave interaction behavior of the RF interaction cavity. The beam-wave interaction process and the bunching phenomenon were described showing the particle preview of the electron beam in which it was found that the electron beam is modulated in the presence of the RF wave. The energy distributions of the particle along the axial length of the cavity show that the net energy transfers to the RF wave. The PIC simulation of the present millimeter wave gyrotron predicted an RF output of ~150 W in the operating $TE_{7,2,1}$ mode at ~260.46 GHz for a DC drive of 15.5 kV, 0.1 A. In addition, thermal and static structural analyses of the present RF cavity have been performed to see the effect of power loss (ohmic loss) on its geometry. The temperature on the inner and outer surfaces of the cavity (straight section) and the corresponding average radial expansion of the cavity were calculated. The magnetic tuning has been done by varying the magnetic field to obtain a tunable bandwidth and that predicted ~1.3 GHz tunable bandwidth. Further, the tunable bandwidth has been enhanced by using the thermal tuning scheme as ~0.58 GHz. The total tunable bandwidth from the combined thermal and magnetic tuning schemes was observed as ~1.88GHz. Therefore, the tuning bandwidth of the present gyrotron is effectively enhanced by ~44.60 % with respect to the magnetic tuning scheme. Further, a single disk window has been designed to extract the output power from the cavity. The window's transfer characteristics show that the window is more transparent for $TE_{7,2,1}$ – $TE_{7,2,4}$ mode from 259.9 GHz – 261.8 GHz, as compared to $TE_{4,3,1}$ mode at ~255.73 GHz and $TE_{2,4,1}$ mode at ~265.58 GHz, respectively. Finally, a single-stage depressor collector has been designed, whose thermal and structural analyses have been performed in ANSYS.